PAPER

The electric double layer at a rutile TiO_2 water interface modelled using density functional theory based molecular dynamics simulation

To cite this article: J Cheng and M Sprik 2014 *J. Phys.: Condens. Matter* **26** 244108

IOP Publishing Journal of Physics: Condensed Matter
J. Phys.: Condens. Matter **26** (2014) 244108 (11pp) doi:10.1088/0953-8984/26/24/244108

The electric double layer at a rutile TiO_2 water interface modelled using density functional theory based molecular dynamics simulation

J Cheng and M Sprik

Department of Chemistry, University of Cambridge, Cambridge CB2 1EW, UK

E-mail: ms284@cam.ac.uk

Received 30 September 2013, revised 22 January 2014
Accepted for publication 28 March 2014
Published 27 May 2014

Abstract

A fully atomistic model of a compact electric double layer at the rutile TiO_2(1 1 0)-water interface is constructed by adding protons to bridging oxygens or removing them from H_2O molecules adsorbed on terminal metal cation sites. The surface charge is compensated by F^- or Na^+ counter ions in outer as well as inner sphere coordination. For each of the protonation states the energy of the TiO_2 conduction band minimum is determined relative to the standard hydrogen electrode by computing the free energy for the combined insertion of an electron in the solid and a proton in solution away from the double layer using density functional theory based molecular dynamics methods. Interpreted as electrode potentials, this gives an estimate of the capacitance which is compared to the capacitance obtained from the difference in the average electrostatic potentials in the solid and aqueous phase. When aligned at the point of zero charge these two methods lead to almost identical potential-charge profiles. We find that inner sphere complexes have a slightly larger capacitance (0.4 F m^{-2}) compared to outer sphere complexes (0.3 F m^{-2}).

Keywords: oxide water interfaces, electric double layers, capacitance, density functional theory

(Some figures may appear in colour only in the online journal)

1. Introduction

Electrical double layers formed at the interface between a metal oxide and an aqueous solution are highly complex environments controlling the chemical reactivity of the surface [1]. Hydrated or hydroxylated metal oxide surfaces act as amphoteric acids. Depending on the value of the pH the surface will either take up protons and become positively charged, or release protons and acquire a negative charge [2]. The charge changes sign at a specific pH characteristic for the surface called the point of zero charge (PZC). The excess or deficit proton charge is compensated by ions of opposite charge in solution building up an electrical double layer (EDL). Experiment can determine the charge density (σ_0) accumulating on the surface as a function of the pH of the bulk solution [3]. However, interpreting such a charging (σ_0 (pH)) curve in terms of a microscopic picture of the charging process is far from straightforward. The problem is that the protonation of the surface not only depends on the intrinsic acidity (pK_a) of surface sites, but also on the potential difference across the EDL and therefore its structure (see figure 1). Microscopic understanding is therefore largely based on empirical surface complexation models (SCM) parametrized to reproduce the experimental data. These models vary in complexity, ranging from 1-pK [4] single site and 2-pK [5] single site models to multi-site models [6]. The acidity models must be complemented by a model of the structure of the EDL determining the capacitance [7, 8].

In view of the indirect and convoluted information provided by experiment, theoretical prediction of intrinsic pKa has become an integral part of colloid and interface science. Several empirical models have been developed, varying in the level of

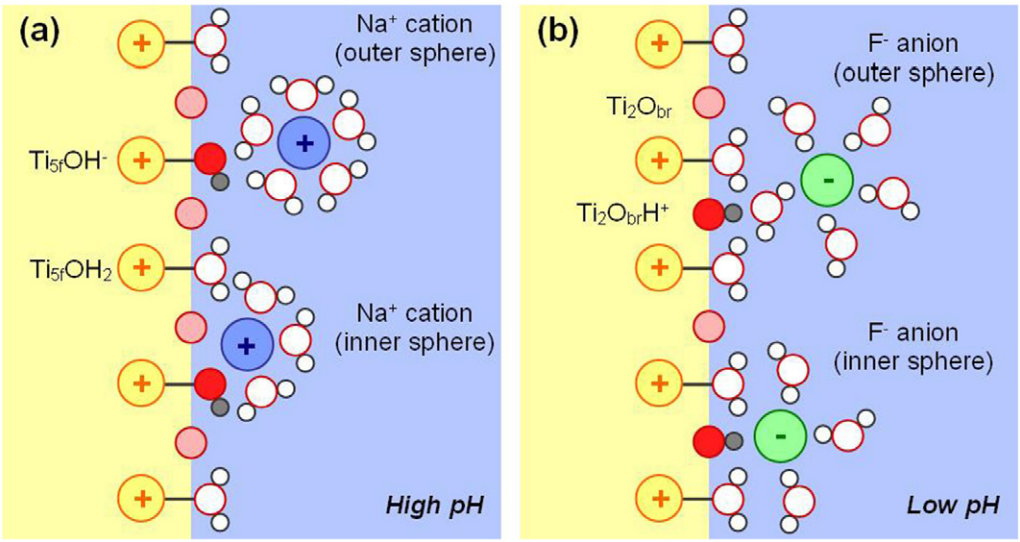

Figure 1. Schematic representation of the Stern layer at a TiO_2 water interface. (*a*) In solutions with a pH higher than the PZC of TiO_2, water molecules adsorbed on terminal five-folded Ti top sites are deprotonated (Ti_{5f} OH_2/ Ti_{5f} OH^-). The oxide surface is negatively charged, attracting cations (Na^+ ions). (*b*) When the pH is lower than the PZC, bridge O atoms are protonated (Ti_2 O_{br} H^+/Ti_2 O_{br}), and the surface is positively charged, attracting anions (F^- ions). Counterions with a full first solvation shell are referred to as outer sphere complexes. If the counterions have given up some water molecules in the first solvation shells to form direct coordination bonds with surface hydroxide groups, they are called inner sphere complexes. The overall charge of the EDL is zero. Charges on oxygens in the solid and water ions have not been indicated.

detail of structural and electronic data required as input for the calculation of the pKa of a site [5, 6, 9, 10]. Recently also the first atomistic computations of intrinsic pKa using force fields [11, 12] and density functional theory (DFT) [13–19] have appeared. Almost all of these studies are under PZC conditions omitting double layer effects. Indeed, including these effects is still a huge challenge. In this contribution we report our first attempt at charging a model metal oxide water interface using the DFT-based molecular dynamics technique (DFTMD) applied in [15] for the computation of the pK_a of a TiO_2 surface (the popular rutile (1 1 0) surface). The DFTMD scheme has been extended for calculation of the one-electron energy levels (band structure) of the solid [20, 21]. Using this method we have computed the change in flat band potential induced by the presence of a Stern layer as schematically indicated in figure 1. Since the surface charge density σ_0 is exactly known (it is imposed) this should give us an estimate of the capacitance of the Stern layer, which can be compared to experiment.

Aqueous TiO_2 is a most popular model system for the mineral/water interface. The first computational studies of TiO_2 covered by mono or bilayers of H_2O molecules date back two decades. For an overview we refer to [22] and citations therein. For applications with an electrochemical background (water oxidation) see [23, 24]. This work has been extended more recently by atomistic simulations of the bulk water interface using force fields [25–29] and DFT-based electronic structure calculation [15, 20, 21, 30–33]. The structure of the layer of adsorbed water and in particular the question of whether the adsorption is associative or dissociative has been an enduring topic subject to some controversy [34, 35]. DFT studies of proton exchange with the bulk solution are more rare. Our computation of the acidity constants of the rutile (1 1 0) surface in [15] is, to the best of our knowledge, the first attempt of such a calculation for aqueous TiO_2 (see also [20]).

The present DFTMD study is a follow-up on our computation of the intrinsic acidity constants at PZC of [15]. The focus is on an exploration of the structure of the compact double layer formed in response to protonation and deprotonation. We have also calculated the capacitance applying two rather different methods. The first is an electrochemical approach involving computation of the potential of the TiO_2 electrode using a method first applied in [36] for the alignment of the band structure of aqueous rutile TiO_2 relative to the standard hydrogen electrode (SHE). The second approach uses the difference in the electrostatic potential in the solid and aqueous phase. The electrostatic perspective is more general and applies to all oxides. Measurement of the electrode potential requires the oxide to be a conductor. As is well known, TiO_2 is the number one model system in photoelectrochemistry with a huge and still growing literature [37]. The TiO_2 -water interface is therefore also an interface between electrochemistry and colloid and interface science [38, 39]. This raises a number of issues, some of which are briefly indicated in the next section. The main purpose of the calculation is, however, practical, namely the comparison of capacitance computed by these two methods. Anticipating our results, the electrode and electrostatic potential method give virtually the same estimate for the capacitance which is, however, lower than experiment by a factor of three.

2. Method

2.1. Experimental and theoretical context

Conventional potentiometric titration measurements are carried out on samples of mineral particles in colloidal suspension,

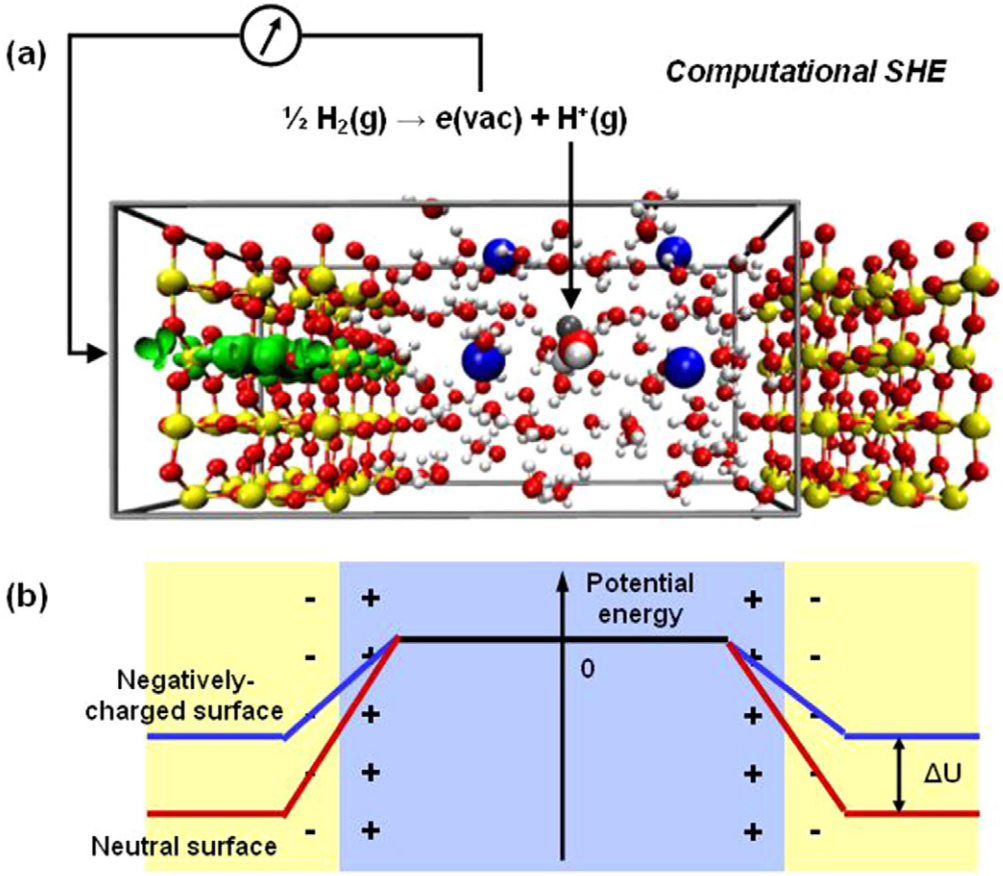

Figure 2. (*a*) Representation of computational SHE construction to compute the electron affinity (conduction band minimum) of TiO_2. Ti, O and H atoms are in yellow, red and white, respectively. The blue balls stand for the EDL counterions. The proton inserted into bulk water is highlighted in grey. The green contour is a spindensity isosurface indicating the electron added to TiO_2. (*b*) Alignment of the electrostatic potential in the solid with respect to bulk water. ΔU is the Hartree potential difference $\varphi_s - \varphi_{aq}$ across the interface. While ΔU cannot be equated with the electrochemical interface potential $\Delta\phi$, changes in the two potentials in response to de(protonation) should be the same.

using an indicator electrode for the determination of the pH [3]. Charging profiles and PZC values for TiO_2 obtained using these methods are available from various sources [40–42]. Some of these data are surface orientation specific. Consulting the compilation of [42] we find a mean estimate of 5.5 for the PZC of the TiO_2 rutile (1 1 0) surface. The DFTMD estimate for this surface we computed in [15] is 3. As mentioned, capacitance can only be estimated indirectly from titration measurements in the form of a parameter in a model of the experimental $\sigma_0(\mathrm{pH})$ curves. Bourikas *et al* [41] give different values for the capacitance C_H of the Stern (Helmholtz) layer for powdered TiO_2 particles, depending on the porosity. We will compare our calculations to the value for compact samples, $C_H = 1\ \mathrm{Fm}^{-2}$ (or 100 $\mu\mathrm{Fcm}^{-2}$).

Potentiometric titration techniques give only very indirect information on interface potentials. TiO_2, however, is a self-doped semiconductor with a good conductivity and can therefore be used as the working electrode in an electrochemical cell. The effect of (de)protonation on the TiO_2 /water interface potential can therefore be monitored by the pH dependence of the open circuit potential U of such a cell. The interface potential, denoted by $\Delta\varphi$, is a sum of the potential difference $\Delta\phi_H$ over the Stern layer and the potential drop $\Delta\phi_{sc}$ over the space charge layer in the semiconductor [43].

$$\Delta\phi = \Delta\phi_H + \Delta\phi_{sc} \tag{1}$$

Provided that $\Delta\phi_{sc}$ is invariant under changes of pH, the response of U to changes in pH can be interpreted as a $\Delta\phi_H(\mathrm{pH})$ curve. This is the basis of the method for surface potential determination developed by Kallay and coworkers [44–46]. It was observed that for H^+ concentrations accessible to experiment the dependence of $\Delta\phi_H$ on pH is to a good approximation linear with a slope proportional to temperature T

$$\frac{\mathrm{d}\Delta\phi_H}{\mathrm{dpH}} = -\alpha\frac{2.3k_BT}{e_0} \tag{2}$$

where k_B is Boltzmann's constant and e_0 is the elementary charge (microscopic units are used). $\alpha = 1$ gives a Nernstian pH dependence [44, 45]. This amounts to a decrease of 59 mV for an increase in pH of one unit.

Alternatively, $\Delta\phi_{sc}$ can be eliminated by application of an appropriate negative bias. The potential where $\Delta\phi_{sc}$ vanishes is called the flatband potential U_{FB}. The capacitance of the depletion layer of a semiconductor is generally much smaller than the capacitance of a Stern layer. U_{FB} can therefore be determined by measuring the dependence of the capacitance on the bias potential (Mott-Schotky plot) [43]. The derivative of U_{FB} with respect to pH satisfies a relation similar to equation (2) with

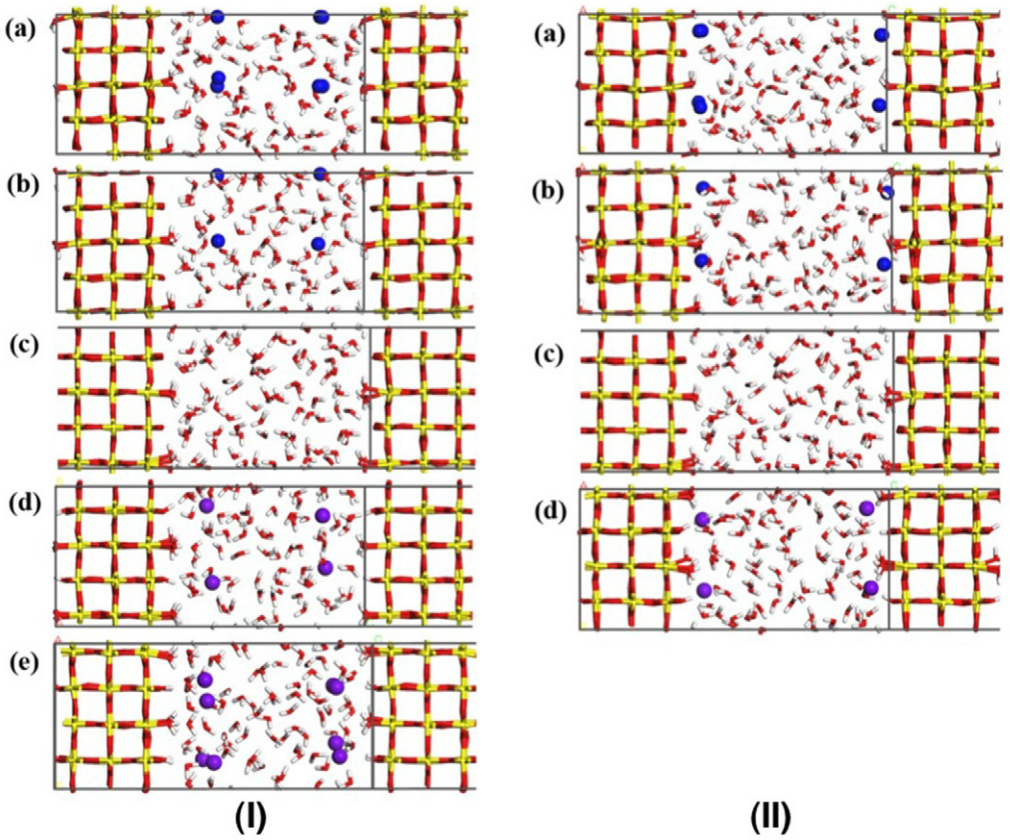

Figure 3. Snapshots of the interface structures of outer sphere (I) and inner sphere (II) complexes at the rutile $TiO_2(110)$ -water interfaces: (*a*) Surface charge density of –0.4 C m^{-2} with 4 Na^+ ions on each surface; (*b*) surface charge density of –0.2 C m^{-2} with 2 Na^+ ions on each surface; (*c*) neutral surface; (*d*) surface charge density of +0.2 C m^{-2} with 2 F^- ions on each surface; and (*e*) surface charge density of +0.4 C m^{-2} with 4 F^- ions on each surface. Ti, O, H, Na and F atoms are in yellow, red, white, blue and purple, respectively.

minimal deviation from Nernstian behaviour ($\alpha = 1$) [47–50]. For TiO_2 the linear Nernstian dependence of the flatband potential is found to persist in a remarkably wide pH window (almost 40 units) [50]. This is in sharp contrast to the ≈20 mV per pH unit decrease ($\alpha = 1/3$) of the open circuit potential for anatase obtained using the Kallay method. [44] (See also the application to hematite ($\alpha - Fe_2O_3$) in [46].)

It is not obvious (at least to the authors of this paper) how to reconcile these seemingly conflicting observations for TiO_2. The main purpose of this brief overview is to point out that our computational method is closer to the electrochemical perspective of the flatband potential than to the interface potential of colloid and interface science. To be precise, what is determined by the calculation is the energy of the conduction band minimum (CBM) of a solid oxide in contact with an electrolytic solution [21] (see also section 2.2). For TiO_2 the gap between the conduction band edge E_{CBM} and Fermi level is small (≈ 0.1 V). The effective electrode potential $U_{CBM} = -E_{CBM}/e_0$ specifying the position of the CBM with respect to some reference electrode is therefore almost equal to potential for the Fermi level under flat band conditions ($U_{CBM} \approx U_{FB}$) .

There is, however, also a crucial difference between our calculation and experiment. The thermodynamic control variable in the calculation is not the activity of the proton in bulk solution (the pH) but the surface charge density σ_0 determined by the fixed protonation state of the surface (see section 2.3). The simulation produces $U(\sigma_0)$ rather than $\sigma_0(\mathrm{pH})$ profiles. The U, σ_0 dependence can be converted to a $\sigma_0(\mathrm{pH})$ charging curve using the appropriate thermodynamic relations with the intrinsic surface acidities and capacitance of the double layer as input parameters. This is the inverse of how SCM's are used for the interpretation of experiment (see also recent work by Björketun and Rossmeisl for an insightful discussion of the status of pH in atomic scale simulation [51, 52]). Such a calculation is way beyond the scope of the present paper. We will focus on the capacitance only which can be immediately obtained from the (absolute) derivative of the computed $U(\sigma_0)$ dependence.

$$C_H^{-1} = \frac{dU_{CBM}}{d\sigma_0} \tag{3}$$

2.2. Calculation of potentials

The model systems used in our method are slabs of solid material separated by a layer of aqueous solution, as illustrated in figure 2(*a*). Full 3D periodic boundary conditions are applied. The central quantity in our scheme is the free energy for reversible insertion of an electron in the solid and a proton in the aqueous solution. The proton is attached to a H_2O molecule in the middle of the aqueous layer where bulk conditions

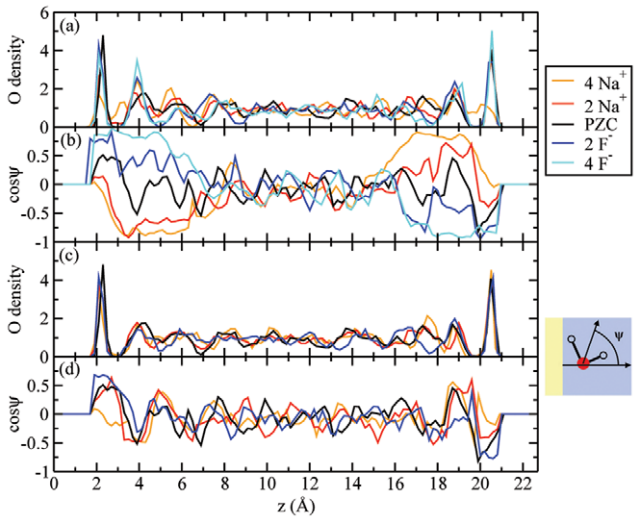

Figure 4. The profile of water density and orientation of outer ((*a*) and (*b*)) and inner ((*c*) and (*d*)) sphere complexes along the z direction normal to the interface. The water density is measured by the density of H_2O oxygen atoms (including surface OH^- for negatively charged surfaces). The orientation of a H_2O molecule is described by $\cos\psi$ where ψ is the angle between the bisector of a H_2O molecule and the normal direction to the surface, as illustrated in the inset. A colour scheme is used to distinguish between surface charge densities indicated by the corresponding number of counterions in the legend.

are assumed to prevail. The free energy for the insertion of the proton electron pair will be indicated by $\Delta A(\mathrm{pbc})_{+\mathrm{H}^+ + e^-}$. The ''pbc'' in brackets is a reminder that the particles are introduced in a periodic system (no interfaces to vacuum). $\Delta A(\mathrm{pbc})_{+\mathrm{H}^+ + e^-}$ is computed using a combination of DFTMD simulation and free energy perturbation methods [21, 53, 54]. The position of the CBM is obtained as an electrode potential $U_{\mathrm{CBM}}(\mathrm{she})$ relative to the SHE according to

$$e_0 U_{\mathrm{CBM}}(\mathrm{she}) = -\Delta A(\mathrm{pbc})_{+\mathrm{H}^+ + e^-} - \mu^{g,\circ}_{\mathrm{H}^+} - \Delta E_{\mathrm{zp}}. \qquad (4)$$

Equation (4) is based on Trasatti's theory of absolute electrode potentials [55, 56]. $\mu^{g,\circ}_{\mathrm{H}^+}$ is the standard chemical potential of the gas-phase proton (H^+ (g)) obtained from the free energy of the reaction $\frac{1}{2}\mathrm{H_2(g)} \rightarrow \mathrm{H^+(g)} + e^-(\mathrm{vac})$. $\mu^{g,\circ}_{\mathrm{H}^+}$ is set equal to the experimental value (15.81 eV). ΔE_{zp} is a correction for the zero point motion of the inserted proton. ΔE_{zp} is estimated from the vibrational density of states of bulk water, giving 0.35 eV. We note that the expression given in our first publication using this method for aligning one-energy levels of solids [36] is marginally different from equation (4) (for a explanation of why we made this adjustment see [54]).

The energy in equation (4) formally corresponds to an adiabatic electron affinity on the SHE scale. The adiabatic electron affinity (EA) and ionization potential (IP) in general differ from the vertical EA and IP for a finite system (molecule). For solids they are the same provided the excess electron or hole occupy extended states. Vertical IPs and EAs can be computed by a variation of our scheme, consisting of vertical addition of an electron and reversible addition (solvation) of the proton carried out in two separated calculations. Substituting the sum of the two insertion energies in equation (4) with the adiabatic energy $\Delta A(\mathrm{pbc})_{+\mathrm{H}^+ + e^-}$ should give the vertical EA. We have checked that the EA computed in this way is indeed equal to the adiabatic EA. This test was performed for rutile TiO_2 at PZC [20, 21]. The value we obtained for U_{CBM} for a model system of similar size and composition used (see below) is –0.4 V versus SHE [20, 21], in good agreement with experiment (–0.35 V versus SHE [49]). This agreement is remarkable because this was a DFT calculation in the generalized gradient approximation (GGA). As is well known, the GGA underestimates band gaps (for TiO_2 by ≈1 eV). Evidently the band gap error predominantly affects the IP of TiO_2, misaligning the VBM rather than the CBM [36].

The correct alignment of the CBM at PZC is a key validation of our method. The capacitance of the EDL can, however, be computed by a more efficient method that avoids the rather expensive computation of the solvation free energy of a proton. This method is based on the change in the average Hartree potential going from the solid to the liquid. Denoting the average Hartree potential in the solid and aqueous phase by φ_{s} and φ_{aq} respectively, the double layer capacitance of equation (3) can be estimated as

$$C_{\mathrm{H}}^{-1} = \frac{\mathrm{d}|\varphi_{\mathrm{s}} - \varphi_{\mathrm{aq}}|}{\mathrm{d}\sigma_0} \qquad (5)$$

Again the absolute value must be used.

As explained in electrochemistry textbooks, $\varphi_{\mathrm{s}} - \varphi_{\mathrm{aq}}$ cannot be identified with the interface potential $\Delta\phi$ of equation (1) (the Galvani potential difference) [56, 57]. A comparison of differences in these quantities is, however, meaningful and the change in the average Hartree potential can be used to estimate a change in $\Delta\varphi$ or the flatband potential, as illustrated in figure 2(*b*). The average Hartree potential is computed by a smoothing procedure. Similar issues regarding determination and interpretation of the average Hartree potential arise in the computation of band offsets at heterojunctions in solids and have been studied in great detail by the computational solid state community [58, 59]. We will in fact apply a smoothing procedure developed in [59]. Further discussion will be deferred to section 3.2 where we present a comparison of estimates of the capacitance using equations (3) and (5)

2.3. Model system and molecular dynamics

The rutile TiO_2(1 1 0)-water interface has been modelled by periodic slabs of three O-Ti-O tri-layers with a volume of water molecules fully filling the space in between. The model unit cell contains therefore two symmetric interfacial planes. To properly represent the oxide surface and bulk water properties, very large supercells with a size of up to 11.9 × 13.2 × 35.8 $Å^3$ containing 48 TiO_2 units and 97 water molecules have been used. Surface charge density is controlled by deprotonating terminal water (negatively charged) or protonating bridge O on the surface (positively charged). The respective counterions (Na^+ and F^-) are placed on top to neutralize the systems. Both inner and outer sphere complexes have been prepared with various surface charge densities (for the cell size we use, one electron charge on the surface

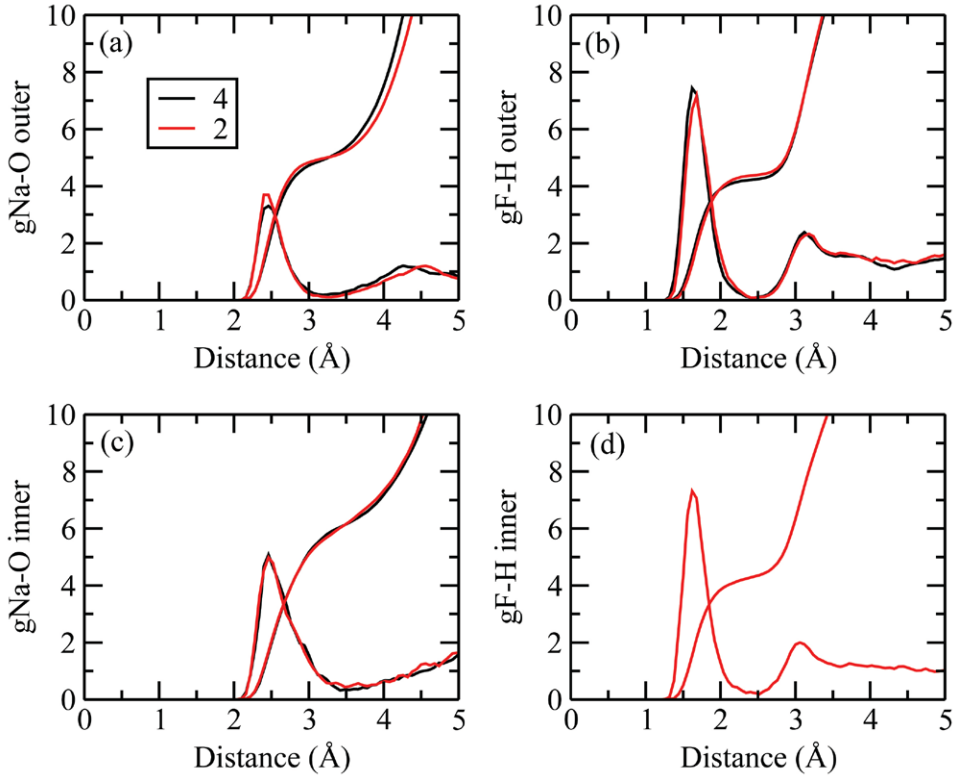

Figure 5. Radial distribution function (RDF) of EDL counterions and solvent H and O atoms (*a*) RDF of Na^+ and O for outer sphere complexes, (*b*) RDF of F^- and H for outer sphere complexes, (*c*) RDF of Na^+ and O for inner sphere complexes, and (*d*) RDF of F^- and H for inner sphere complexes. Black and red curves are for 4 and 2 ions adsorbed on the surface, corresponding to charge density ±0.4 C m^{-2} and ±0.2 C m^{-2}, respectively. The monotonically rising curves of the same colour are the corresponding accumulative coordination numbers (the scale is the same as for the normalized RDF).

corresponds to 0.1 C m^{-2}) and further equilibrated using MD runs. Snapshots of the interface structures are shown in figure 3.

Born Oppenheimer DFTMD simulations were carried out using the freely available program package CP2K/Quickstep [60, 61]. The 2s, 2p electrons of the O atoms and the 3s, 3p, 4s, 3d electrons of the Ti atoms were treated as valence. The basis sets were double-ζ basis functions with one set of polarization functions [62]. The plane wave cutoff for the density is 280 Ry. The core electrons are represented by analytic Goedecker–Teter–Hutter pseudopotentials [63, 64]. The Perdew–Burke–Ernzerhof functional is used. The time step for the MD runs is 0.5 fs. Canonical ensemble conditions were imposed by a Nos é -Hoover thermostat with a target temperature of 330 K. In MD runs, 1 ∼ 2 ps of equilibration period was followed by 5 ∼ 10 ps of production period. The same settings were applied before, and more detailed descriptions can be found in our previous publications [15, 36]. It is important that the simulations are carried out in a fixed and well-defined protonation state. Therefore all O-H bonds in water molecules, including those adsorbed on the surface, are constrained by harmonic springs to prevent dissociation.

As has been pointed out repeatedly, the structure and adsorption properties of TiO_2 surfaces oscillate with the thickness of the model system slab [22, 31]. Moreover our solid samples have two surfaces, both with an EDL. Three tri-layers may not be large enough to screen the interaction between these EDLs. An even larger size model consisting of five tri-layers of TiO_2 and 97 water molecules was constructed and we repeated the calculation for the neutral surface and negatively charged surface with a charge density of −0.2 C m^{-2} (2 Na^+ ions on each surface forming inner sphere complexes). We verified that three and five layer models give almost the same potential differences across the interface for both neutral and charged surfaces. This suggests that the three layer model should be sufficient for the calculation of interface potentials (at least in first approximation).

3. Results

3.1. Interface structure

The electrostatic properties of a solid liquid interface are ultimately determined by its structure. MD trajectories should in principle contain all the relevant structural detail. An informative probe of the order and size of an EDL is the profile of the water density and orientation along the direction normal to the surface (z axis). We first discuss the structure at PZC and use this a reference for the investigation of the effect of charging the EDL. Figure 4 shows the O density of water molecules and the cosine of the angle between the bisector of a water molecule and z axis (cosψ). We also compare inner and outer sphere complexes. It can be seen from the O density profiles that there are two distinct peaks at ∼2.2 Å and ∼3.9 Å, corresponding to a layer of water molecules chemisorbed at terminal Ti sites and a second layer adsorbed on top of the first

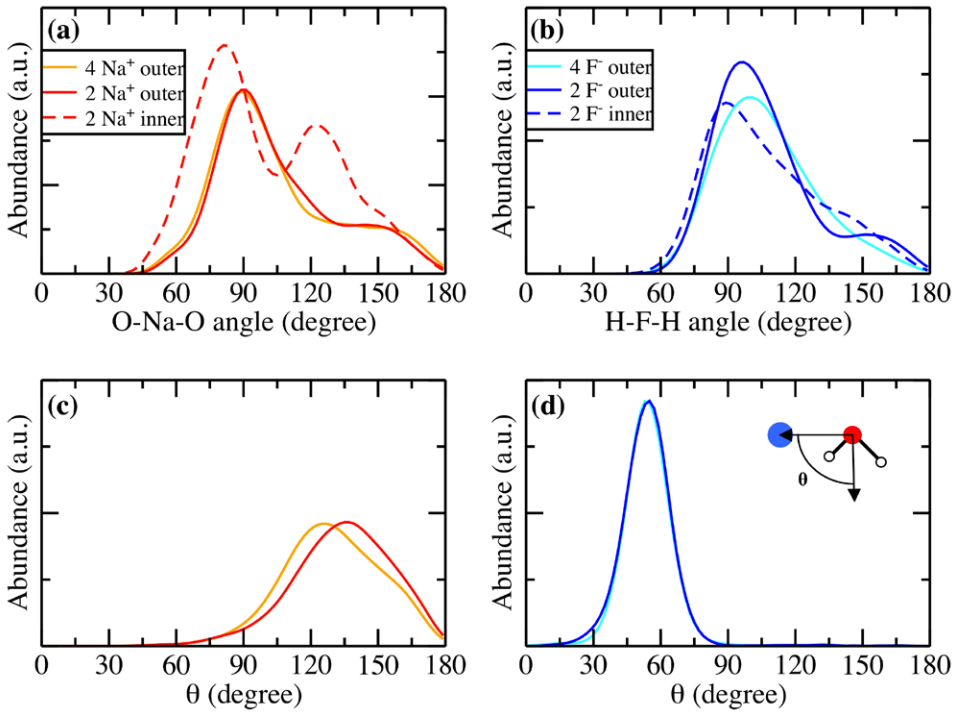

Figure 6. Geometry of the first solvation shell of the EDL counterions. (*a*) and (*b*) show the distribution of O-Na-O angles and H-F-H angles, respectively. (*c*) and (*d*) show the distribution of the angle θ between the bisector of the water molecule and the radial direction (see the inset). The colour code in panels (*c*) and (*d*) is the same as in panels (*a*) and (*b*).

layer. These results are consistent within a 0.1 Å margin with recent crystal truncation rod measurements and force field MD simulations [25–27].

Net surface charge and counterions disturb the water density profile established at PZC, as has been observed in x-ray reflectivity experiments [25]. Because of the limitations in time scale and cell size, our DFTMD simulations may not reliably resolve all the subtle rearrangements in the water density profiles. However, our results show that in response to deprotonation a new peak appears in between the first and second peaks for outer sphere complexes (see orange and red curves in figure 4(*a*)). We interpret this observation as an indication of desorption of surface water. When the surface charge density has decreased to -0.4 C m^{-2}, all water molecules desorb. The residual first peak is related to the terminal OH^- group on the Ti top sites (see the structure in figure 3I(*a*)).

The effect of charging on the water orientation is even more pronounced, as shown in figures 4(*b*) and (*d*). Particularly sensitive is the orientation in the interfacial region of outer sphere complexes. At PZC, water molecules chemisorb on terminal Ti sites with H atoms and the dipole vector pointing slightly upwards, while the water molecules in the second layer turn the H atoms towards the surface to form hydrogen bonds with bridging O atoms. The water dipole vectors in the first layer of positively charged surfaces almost point straight up, with maximum cosψ breaking the hydrogen bonding in the inner plane. Even the water molecules in the second layer turn around, also pointing the dipole vectors upwards. On the other hand, when the surface becomes negatively charged, electrostatic interaction forces the water molecules to point the H atoms downwards. As can be seen in figure 4(*b*) (red and orange curves), cosψ values associated with the first water layer are substantially reduced. For low charge density the chemisorbed water molecules lie flat on the surface, and become desorbed with increasing negative charge density, as has been seen previously in O density profiles. For inner sphere complexes, the change in the water dipole profiles is less dramatic. One clear feature seen from figure 4(*d*) is that cosψ is again enhanced by positive surface charge, implying small values of ψ, and vice versa. Different from outer sphere complexes for highly negatively charged surfaces, the chemisorbed water molecules do not desorb from the surface; rather they reorient to form coordination bonds with Na^+ ions, as shown in figure 3II(*b*).

Next we discuss the solvation structure of the counterions. For inner sphere complexes, both Na^+ and F^- ions are located between the first and second water layers at an average distance of around $z = 2.8$ Å and $z = 3.6$ Å from the TiO_2 surface. The position of ions in outer sphere complexes is less localized, varying between $z = 6.2 \sim 6.7$ Å and $5.0 \sim 6.0$ Å, respectively. The radial distribution function (RDF) for the counterions is shown in figure 5. It is interesting to find that Na^+ ions form six coordination bonds with O atoms for inner sphere complexes, one more than outer sphere complexes and solvated ions in bulk water [65]. The first peak position in the Na^+-O RDF moves out by 0.1 Å, from 2.4 Å to 2.5 Å, to accommodate the extra ligand. The coordination number (CN) of F^- ions and the first peak position in the RDF hardly differ between inner and outer sphere complexes (see figure 5). The small change we found is that the CN decreases slightly by 0.2 when the surface charge density increases from 0.2 to 0.4 C m^{-2}. This is consistent with a small peak observed at about 160 degrees in the distribution of H-F-H angle (see

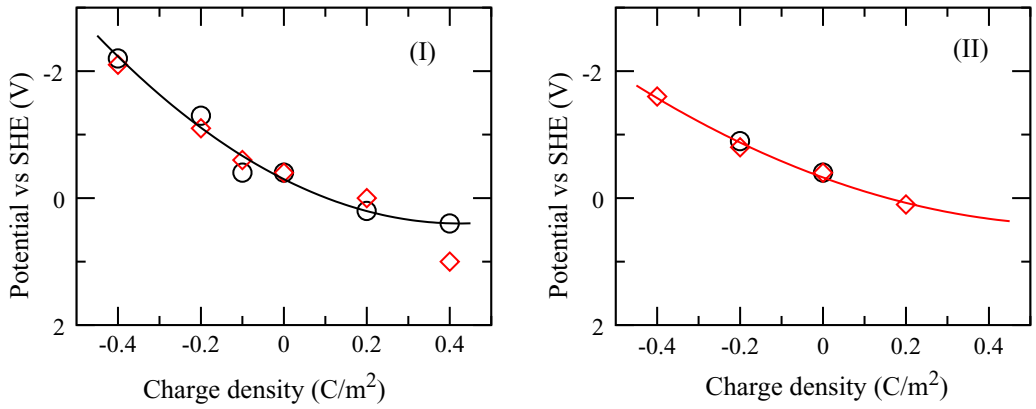

Figure 7. Potential-surface charge density curves for double layers with counterions in outer (I) and inner (II) sphere complexation (see figure 3). Black circles give the position of the conduction band minimum of TiO_2 computed as a potential versus SHE according to equation (4). The red diamonds are the corresponding differences in the average electrostatic potential (see figure 8) aligned with the electrode potential at the point of zero charge. The drawn curves are quadratic fits used to determine the differential capacitance.

figure 6(*b*) for charge density 0.2 C m^{-2}, which is a signature of the five-coordinated square pyramidal structure.

Another structural parameter probing the perturbation of ion solvation by the electric field in the EDL is the angle φ between the water dipole vector and the radial vector pointing from the O atom in first solvation shell to the ion. According to figures 6(*c*) and (*d*), the distribution of φ shifts towards smaller angles when the negative charge builds up. This must be the effect of water dipoles aligning themselves to the direction of the electric field normal to the surface. In contrast, the solvation shell of F^- is more directional, with a narrow distribution of φ, and therefore no shift is observed.

3.2. Band alignment and capacitance

One-electron energy levels can be specified with respect to vacuum or using the SHE as reference. The first approach requires a model system with an interface to vacuum, the second a computational hydrogen electrode. As outlined in section 2.2, we have adopted the electrochemical approach and computed the effective electrode potential $U_{\mathrm{CBM}}(\mathrm{she})$ of the CBM of TiO_2 relative to the SHE according to equation (4). This calculation was carried out for a subset of six double layer model systems of figure 3 by inserting an electron and a proton into each of these systems. The result is shown in figure 7. At maximum deprotonation (σ_0 = –0.4 C m^{-2}) the CBM has been lifted by 2 V above the position at PZC. The charging is not quite symmetric. The $U_{\mathrm{CBM}}(\sigma_0)$ profiles are not straight but slightly curved. As a result the capacitance C_{H} as defined in equation (3) varies with the protonation state and should be interpreted as a differential capacitance. C_{H} for negatively charged (deprotonated) surfaces is found to be slightly lower than for positively charged (protonated) surfaces. This is in line with the general chemical intuition that F^- anions have a larger radius and a more weakly bound solvation shell, leading to a higher dielectric constant of water within the EDL and thus a higher capacitance.

The computational hydrogen electrode uses the solvation free energy of the proton as energy reference. The sampling over solvent fluctuations required for the determination of this quantity makes the computation of $U_{\mathrm{CBM}}(\mathrm{she})$ very expensive. Interface potentials are likely to be less sensitive to solvent fluctuations and the electrostatic potential alignment method (equation (5)) can be expected to be a more efficient scheme for computation of the interface capacitance. Recall that the φ_{s} and φ_{aq} in equation (5) are meant to be average potentials in the bulk solid (TiO_2) and aqueous phases, respectively. In applications to heterojunctions in solids this average is computed by a coarse graining procedure that washes out microscopic structure due to the underlying periodic lattice in solids [59]. The smoothing must, however, be restricted to some local environment in order to be able to describe the gradient across an interface.

In our calculation we have used the nanosmoothing scheme of [59] as implemented in the MACROAVE code [59]. The result for the model TiO_2 water interface is shown in figure 8 along with the original potential profile before smoothing. In the interior of the TiO_2 slab, even though only three layers wide, the procedure works as it is designed to do, removing the huge spikes in the atomic regions. These spikes are much smaller in the aqueous part of the supercell. This is an effect of the disorder in the liquid. The potential shown in figure 8 is that of an instantaneous configuration. There is hardly any signature of atomic structure except perhaps near the interface with the solid. Instead the potential fluctuates in an irregular pattern with a variance of less than 5 V. When averaged over a DFTMD run the dynamical fluctuations will further reduce the spatial modulation, ideally eliminating it completely in a converged run.

The results shown in figure 8 suggest that nanosmoothing of the electrostatic potential of a small set of equilibrated configurations should give already a good estimate of φ_{aq}. Substituting in equation (5) we should therefore obtain an estimate of capacitance at a fraction of the cost of the computational hydrogen electrode method. The question now, of course, is: are these two estimates the same? As mentioned, alignment of the Hartree potentials in two phases cannot be used to compute the interface potential $\Delta\phi$ (equation (1)). Indeed, the 9 V for $\varphi_{\mathrm{aq}}-\varphi_{\mathrm{s}}$ in figure 8 is an unrealistically high potential in electrochemistry. Therefore, to compare to the σ_0 dependence of $U_{\mathrm{CBM}}(\mathrm{she})$ we simply set $\varphi_{\mathrm{aq}}-\varphi_{\mathrm{s}} = U_{\mathrm{CBM}}(\mathrm{she})$

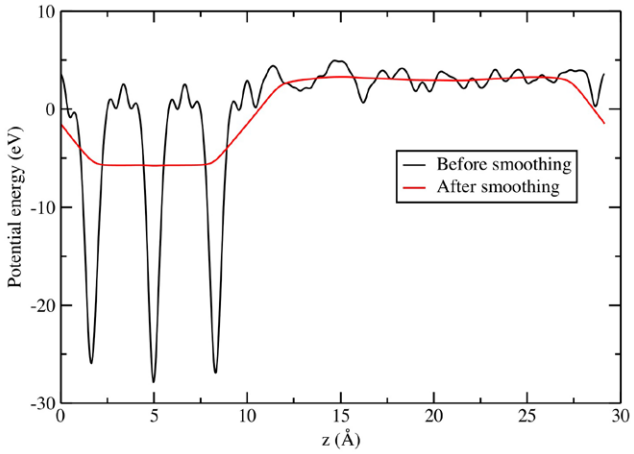

Figure 8. The profile of electrostatic potential along the z direction normal to the interface averaged over the two in plane coordinates x and y. The black curve is calculated from one snapshot of the MD trajectory of the neutral TiO_2 water interface model. The potential spikes come from the nuclear charges of Ti and O atoms in TiO_2. The red curve is obtained after applying a smoothing procedure in which the spikes are effectively removed.

at $\sigma_0 = 0$, obtaining the second curve in figure 7. The two sets of data points coincide within the statistical uncertainty of the calculation. The consistency of the results of these two very different methods is a strong validation of both methods.

While neither of the two methods can give us the electrochemical (Galvani) interface potential $\Delta\varphi$ of equation (1) we can use the σ_0 profiles in figure 7 to estimate the capacitance C_H. Taking the derivative at PZC, the capacitance for the EDL with outer sphere complexes as counter charge is 0.30 F m^{-2}. Inner sphere coordination gives a somewhat higher value $C_H = 0.42$ F m^{-2}. The calculated capacitance is about a third of the experimental estimate of $C_H = 1$ F m^{-2} of [41] (see section 2.1). Note, however, the 0.5 F m^{-2} uncertainty in the experimental estimate.

4. Evaluation and outlook

The DFTMD structure of the interface and double layer as discussed in section 3.1 is in broad agreement with the available experimental data. We can clearly observe that charging has a drastic effect on the structure of the interface. Water molecules in the EDL are forced to align their dipoles with the electric field. This reorientation strongly interferes with the intermolecular hydrogen bonding. For very negative surface charge, this effect can even lead to desorption from terminal Ti sites. The hydration of counterions is also distorted, as is reflected in changes in the coordination number and water orientation. For instance, Na^+ ions forming inner sphere complexes have six H_2O molecules in the first shell, one more than in outer sphere complexes and bulk water. The perturbation of solvation structure appears to be more pronounced for Na^+ than F^- ions, presumably because of differences in rigidity and directionality of the H_2O coordination.

The capacitance was computed by two alternative methods: by determining the energy of the conduction band edge of TiO_2 using a computational hydrogen electrode and also by comparing the average electrostatic potentials in the solid and aqueous electrolyte. These two rather different methods led to virtually the same capacitance. The Hartree potential alignment method is the more conventional and certainly the more efficient method. However, it only gives the shifts in energy levels, while the computational hydrogen electrode method also gives their absolute positions. A similar approach is used in [51] and [52]. Absolute positions can also be computed from the electronic workfunctions in systems with an vacuum interface [66, 67]. Again this is significantly cheaper than the combined insertion of electrons and protons. These methods must, however, be seen in a broader context. Proton insertion can be equally used to compute surface acidity [15, 17–19] and the reversible potentials for the oxidative dehydrogenation of adsorbed water [20]. Proton insertion is the key to consistent calculation of the equilibrium constants for the deprotonation coupled oxidation and protonation coupled reduction reactions controlling the (photo)electrochemical and charge storage properties of transition metal oxides. This was for us the motivation for adopting these methods.

Capacitance is a hard number to directly compare to experiment. The calculated capacitance reported in section 3.2 is too small by a factor of about three. However, in the construction of our first DFTMD model of a charged oxide water interface we have made a number simplifications, making the comparison to experiment rather ambiguous. The simplifications were forced on us because of the severe limitations in the size of DTMD model systems. We will briefly recapitulate what has been ignored in our calculation but will in reality contribute to the capacitance measured in experiment.

A minimum model of the EDL at a semiconductor liquid junction (SCLJ) is partitioned in three zones: the diffuse layer, the compact (Stern) double layer and the space charge region. The capacitance of these three zones are put in series; hence the smallest of the three dominates. What is computed in our method is the capacitance of the Stern layer (C_H) only. The diffuse layer on the electrolyte side and the space charge layer on the solid side of the interface are completely missing in our model systems. We argued that at the high ionic strength relevant in colloidal science the capacitance of the diffuse layer is significantly larger than the capacitance of the Stern layer and therefore can be omitted in first approximation. However, eliminating the salt all together, what we have done, seems a drastic approximation. After this first exploration we now see a possibility to include salt in the water compartment, even for the DFTMD system sizes we can afford, although in a somewhat different system geometry than that used here. This will be the main focus of the continuation of the project.

The capacitance of space charge layers is small and will determine in practice the capacitance of a SCLJ. In view of the huge width of a space charge layer (hundreds of nanometers) it is impossible to account for this effect in atomistic modelling. The implication is that our simulation can only be compared to systems under flatband conditions. This can already be instructive for an analysis of band alignment and catalysis, as we have shown in [20]. For the understanding of capacitance, the restriction to flatband conditions is more of handicap. For example, it prevents direct computation of the coefficient α in equation (2) because a change in potential

in general has an effect on the band bending. Some of these issues can be resolved by calculations of metallic oxides such as RuO_2. A further consideration for the comparison to experiment is that the model system exposes a surface with a single orientation (1 1 0) to solution, while the experimental result probably applies to a mixture of several stable orientations. The adsorption of coions is also ignored in the calculation. Because of these uncertainties we have postponed a more detailed structural analysis of the result for capacitance, considering it premature at this stage. Viewed as a feasibility study, we are inclined to regard the 30 to 40 μFcm^{-2} estimate we obtain as encouraging. This still is a relatively large capacitance in the range of what is expected for hydrated/hydroxylated oxides.

In conclusion, in spite of system size limitations we believe that atomistic simulation opens up interesting possibilities in the modelling of electric double layers of oxides. To make this point we return to the issue raised in the brief overview of experiment in section 2.1. The TiO_2 -water interface is studied in colloid and surface science as well as electrochemistry, but from a somewhat different perspective. Colloid and interface science tends to see TiO_2 as another example of a mineral oxide exchanging protons with the solution. Electrochemical processes naturally involve electron transfer. Metallic and semiconducting transition metal oxides can do both. They absorb charge in response to a change of pH (titration) and to a change of electrode potential. For sufficiently large conductivity the change in charge can be measured by a range of electrochemical methods (Voltammetry, electrochemical impedance spectroscopy) [38, 39]. The capacitance of these systems has therefore an electric double layer (non-Faradaic) and pseudo capacitance (Faradaic) component [68–70]. Similarly, TiO_2 anodes in Li batteries exhibit pseudo capacitance behaviour when adsorbing/intercalating Li^+ ions [71, 72]. The situation for H^+ is less clear. However [48] and [50] make the case that the adsorption of H^+ on TiO_2 can also be Faradaic. This should perhaps be taken into account when interpreting the pronounced sub-Nernstian behaviour of the potential-pH curve ($\alpha < 1$ in equation (2)) observed by Kallay and coworkers [44].

Our computational hydrogen electrode method, unifying calculation of acidity constants and redox potentials, is well suited to address these issues. A first task would be to study (de)protonation under constant potential (potentiostatic) conditions. Related to this is the determination of the surface Pourbaix diagram, taking into account not only neutral [23, 24] but also charged phases. The ultimate aim would be to compute the α parameter in equation (2) under the general conditions of equilibrium proton coupled electron exchange.

Acknowledgments

JC is grateful for financial support from Emmanuel College Cambridge and the Engineering and Physical Sciences Research Council (EPSRC) of the United Kingdom. We also acknowledge support from the UKCP consortium for access to HECToR, the UK's high-end computing resource funded by the Research Councils.

References

[1] Brown G E *et al* 1999 *Chem. Rev.* **99** 77–174
[2] Stumm W 1992 *Chemistry of the Soil–Water Interface* (New York: Wiley)
[3] Lützenkirchen J, Preocanin T, Kovacevic D, Tomisic V, Lövgren L and Kallay N 2012 *Croat. Chem. Acta* **85** 391–417
[4] Van Riemsdijk, W H , Bolt G H, Koopal L K and Blaakmeer J 1986 *J. Colloid Interface Sci.* **109** 219–28
[5] Sverjensky , D A and Sahai N 1996 *Geochim. Cosmochim. Acta* **60** 3773–97
[6] Hiemstra T, Van Riemsdijk W H and Bolt G H 1989 *J. Colloid Interface Sci.* **133** 91–104
[7] Sahai N and Sverjensky D A 1997 *Geochim. Cosmochim. Acta* **61** 2801–26
[8] Hiemstra T and Riemsdijk W H V 2006 *J. Colloid Interface Sci.* **301** 1–18
[9] Hiemstra T, Venema P and Riemsdijk W H V 1996 *J. Colloid Interface Sci.* **184** 680–92
[10] Bickmore B R, Tadanier C J, Rosso K M, Monn W D and Egget D L 2004 *Geochim. Cosmochim. Acta* **68** 2025–42
[11] Rustad J R, Wasserman E, Felmy A R and Wilke C 1998 *J. Colloid Interface Sci.* **198** 119–29
[12] Rustad J R, Wasserman E and Felmy A R 1999 *Surf. Sci.* **424** 28–35
[13] Leung K, Nielsen I M B and Criscenti L J 2009 *J. Am. Chem. Soc.* **131** 18358–65
[14] Leung K and Criscenti L J 2012 *J. Phys.: Condens. Matter* **24** 124105
[15] Cheng J and Sprik M 2010 *J. Chem. Theor. Comput.* **6** 880–9
[16] Sulpizi M, Gaigeot M-P and Sprik M 2012 *J. Chem. Theor. Comput.* **8** 137–47
[17] Tazi S, Rotenberg B, Salanne M, Sprik M and Sulpizi M 2012 *Geochim. Cosmochim. Acta* **94** 1–11
[18] Liu X, Lu X, Sprik M, Cheng J, Meijer E J and Wang R 2013 *Geochim. Cosmochim. Acta* **117** 180–90
[19] Liu X, Cheng J, Sprik M, Lu X and Wang R 2013 *Geochim. Cosmochim. Acta* **120** 487–95
[20] Cheng J, Sulpizi M, VandeVondele J and Sprik M 2012 *ChemCatChem* **4** 636–40
[21] Cheng J and Sprik M 2012 *Phys. Chem. Chem. Phys.* **14** 11245–67
[22] Kowalski P M, Meyer B and Marx D 2009 *Phys. Rev.* B **79** 115410
[23] Rossmeisl J, Qu Z-W, Zhu H, Kroes G-J and Nørskov J K 2007 *J. Electroanal. Chem.* **607** 83–9
[24] Li Y-F, Liu Z-P, Liu L and Gao W 2010 *J. Am. Chem. Soc.* **132** 13008–15
[25] Zhang Z *et al* 2004 *Langmuir* **20** 4954–69
[26] Predota M, Bandura A V, Cummings P T, Kubicki J D, Wesolowski D J, Chialvo A A and Machesky M L 2004 *J. Phys. Chem.* B **108** 12049
[27] Predota M, Zhang Z, Fenter P, Wesolowski D J and Cummings P T 2004 *J. Phys. Chem.* B **108** 12061–72
[28] Machesky M L *et al* 2008 *Langmuir* **24** 12331–9
[29] Nakamura H, Ohto T and Nagata Y 2013 *J. Chem. Theor. Comput.* **9** 1193–1201
[30] Cheng H and Selloni A 2010 *Langmuir* **26** 11518–25
[31] Liu L-M, Zhang C, Thornton G and Michaelides A 2010 *Phys. Rev.* B **82** 161415
[32] Sumita M, Hu C and Tateyama Y 2010 *J. Phys. Chem.* C **114** 18529–37
[33] De Angelis F, Fantacci S and Gebauer R 2011 *J. Phys. Chem. Lett.* **2** 813–7
[34] Wesolowski D J *et al* 2012 *Phys. Rev.* B **85** 167401
[35] Liu L-M, Zhang C, Thornton G and Michaelides A 2012 *Phys. Rev.* B **85** 167402

[36] Cheng J and Sprik M 2010 *Phys. Rev.* B **82** 081406
[37] Fujishima A, Zhang X and Tryk D A 2008 *Surf. Sci. Rep.* **63** 515–82
[38] Ardizzone S and Trasatti S 1996 *J. Colloid Interface Sci.* **64** 173–251
[39] Trasatti S 1999 *Interfacial Electrochemistry: Theory, Experiment and Applications* Wieckowski A (New York: Marcel Dekker)
[40] Yates D E and Healy T W 1980 *J. Chem. Soc. Faraday Trans.* I **76** 9–18
[41] Bourikas K, Hiemstra T and Van Riemsdijk W H 2001 *Langmuir* **17** 749–56
[42] Kosmulski M 2011 *J. Colloid Interface Sci.* **353** 1–15
[43] Gerischer H 1997 *The CRC Handbook of Solid State Electrochemistry* Gellings P J and Bouwmeester H J M (Boca Raton, FL: CRC press)
[44] Kallay N, Preocanin T and Ivsic T 2007 *J. Colloid Interface Sci.* **309** 21–7
[45] Zarzycki P, Rosso K, Chatman S, Preocanin T, Kallay N and Piasecki W 2010 *Croat. Chem. Acta* **83** 457–74
[46] Chatman S, Zarzycki P and Rosso K 2013 *Phys. Chem. Chem. Phys.* **15** 13911–21
[47] Gerischer H 1989 *Electrochim. Acta* **34** 1005–9
[48] Matsumoto Y, Yoshikawa T and Sato E 1989 *J. Electrochem. Soc.* **136** 1389–91
[49] Kavan l, Grätzel M, Gilbert S E, Klemenz C and Scheel H J 1996 *J. Am. Chem. Soc.* **118** 6716
[50] Lyon L A and Hupp J T 1999 *J. Phys. Chem.* B **103** 4623–8
[51] Rossmeisl J, Skúlason E, Björketun M E, Tripkovic V and Nørskov J K 2008 *Chem. Phys. Lett.* **466** 68–71
[52] Rossmeisl J, Chan K, Ahmed R, Tripkovic V and Björketun M E 2013 *Phys. Chem. Chem. Phys.* **15** 10321–5
[53] Cheng J, Sulpizi M and Sprik M 2009 *J. Chem. Phys.* **131** 154504
[54] Costanzo F, Della Valle R G, Sulpizi M and Sprik M 2011 *J. Chem. Phys.* **134** 244508
[55] Trasatti S 1986 *Pure Appl. Chem.* **58** 955–66
[56] Fawcett W R 2004 *Liquids, Solutions, and Interfaces* (Oxford: Oxford University Press)
[57] Pethica B A 2007 *Phys. Chem. Chem. Phys.* **9** 6253–62
[58] Franciosi A and VandeWalle C G 1996 *Surf. Sci. Rep.* **25** 1–140
[59] Junquera J, Cohen M H, Rabe and K M 2007 *J. Phys.: Condens. Matter* **19** 213203
[60] The CP2K developers group 2008 (www.cp2k.org)
[61] VandeVondele J, Krack M, Mohamed F, Parrinello M, Chassaing T and Hutter J 2005 *Comput. Phys. Commun.* **167** 103–28
[62] VandeVondele J and Hutter J 2007 *J. Chem. Phys.* **127** 114105
[63] Goedecker S, Teter M and Hutter J 1996 *Phys. Rev.* B **54** 1703
[64] Hartwigsen C, Goedecker S and Hutter J 1998 *Phys. Rev.* B **58** 3641
[65] White J A, Schwegler E, Galli G and Gygi F 2000 *J. Chem. Phys.* **113** 4668–73
[66] Taylor C D, Wasileski S A, Filhol J-S and Neurock M 2006 *Phys. Rev. B* **73** 165402
[67] Sugino O, Hamada I, Otani M, Morikawa Y, Ikeshoji T and Okamoto Y 2007 *Surface Sci.* **601** 5237
[68] Conway B E 1999 *Electrochemical Supercapacitors* (New York: Plenum)
[69] Liu Y, Zhou F and Ozolins V 2012 *J. Phys. Chem.* C **116** 1450–7
[70] Ozolins V, Zhou F and Asta M 2013 *Acc. Chem. Res.* **46** 1084–93
[71] Wang J, Polleux J, Lim J and Dunn B 2007 *J. Phys. Chem.* C **111** 14925–31
[72] Kang J, Wei S-H, Zhu K and Kim Y-H 2011 *J. Phys. Chem.* C **115** 4909–15